JBC RESEARCH ARTICLE

The disordered protein SERF promotes α-Synuclein aggregation through liquid–liquid phase separation

Received for publication, March 1, 2023, and in revised form, December 26, 2023 Published, Papers in Press, January 23, 2024,
https://doi.org/10.1016/j.jbc.2024.105667

He-Ning Liu[1,‡], Ting Wang[1,‡], Jin-Jian Hu[2,‡], Long Chen[1], Xiangyan Shi[3,*], Yan-Mei Li[2,*], and Shi-Zhong Luo[1,*]

From the [1]Beijing Key Laboratory of Bioprocess, College of Life Science and Technology, Beijing University of Chemical Technology, Beijing, China; [2]Key Lab of Bioorganic Phosphorus Chemistry & Chemical Biology, Department of Chemistry, Tsinghua University, Beijing, China; [3]Department of Biology, Shenzhen MSU-BIT University, Shenzhen, China

Reviewed by members of the JBC Editorial Board. Edited by Ursula Jakob

The aggregation of α-Synuclein (α-Syn) into amyloid fibrils is the hallmark of Parkinson's disease. Under stress or other pathological conditions, the accumulation of α-Syn oligomers is the main contributor to the cytotoxicity. A potential approach for treating Parkinson's disease involves preventing the accumulation of these α-Syn oligomers. In this study, we present a novel mechanism involving a conserved group of disorderly proteins known as small EDRK-rich factor (SERF), which promotes the aggregation of α-Syn through a cophase separation process. Using diverse methods like confocal microscopy, fluorescence recovery after photobleaching assays, solution-state NMR spectroscopy, and Western blot, we determined that the N-terminal domain of SERF1a plays a role in the interactions that occur during cophase separation. Within these droplets, α-Syn undergoes a gradual transformation from solid condensates to amyloid fibrils, while SERF1a is excluded from the condensates and dissolves into the solution. Notably, *in vivo* experiments show that SERF1a cophase separation with α-Syn significantly reduces the deposition of α-Syn oligomers and decreases its cellular toxicity under stress. These findings suggest that SERF1a accelerates the conversion of α-Syn from highly toxic oligomers to less toxic fibrils through cophase separation, thereby mitigating the biological damage of α-Syn aggregation.

Amyloids with distinct cross beta-sheet structures are the key characteristic of neurodegenerative diseases. Several classical examples include mutant huntingtin in Huntington disease, amyloid beta and tau in Alzheimer disease, and α-Synuclein (α-Syn) in Parkinson disease (PD) (1–5). The destabilization of protein folded state, due to the unbalance of cellular microenvironment, including various biochemical, cytological, and physiological perturbations, is potentially one of the main factors to trigger the protein aggregation to form the oligomers and fibrils (6–11), which result in the dysregulation of biological processes (12). Nowadays, an increasing number of evidences show that α-Syn fibrils are unlikely the primary neurotoxic species in PD and the principal toxicity is from the α-Syn oligomers (13, 14). Several studies indicate that the oligomers accumulate as the intermediates in the polymerization of α-Syn fibrils and interfere with lipid membranes and membrane-associated processes (15, 16). Furthermore, α-Syn oligomers bind to the proteasome, inhibiting its hydrolytic activity, which disrupts protein degradation pathways and hampers the clearance of misfolded proteins (17). In addition, the accumulation of α-Syn oligomers in the endoplasmic reticulum triggers the endoplasmic reticulum stress response (18) and they also interact with mitochondrial complex I, contributing to mitochondrial dysfunction (19). Collectively, these factors contribute to an increased protein burden within cells, ultimately resulting in cell death. Therefore, preventing the accumulation of α-Syn oligomers can be a potential strategy to inhibit PD pathogenesis.

α-Syn aggregation proceeds through the secondary nucleation mechanism, with the extremely slow lag phase of primary nucleation, representing the crucial bottleneck step and causing the accumulation of oligomeric species (20). Consequently, the modulation of α-Syn aggregation stands as a pivotal strategy for reducing cytotoxicity (21–23). It has been reported that liquid–liquid phase separation (LLPS) mediates the primary nucleation, which is a key step for inducing pathological aggregation of α-Syn (9). Posttranslational modifications and pathological mutations may trigger abnormal protein phase separation to initiate amyloid assembly (24–26). In addition, cellular turmoil in pH, metal ions, or other cell stresses (temperature, rotenone) can affect protein phase separation behaviors (27–29), which promotes α-Syn converting from soluble form to solid aggregation (9, 30, 31). Therefore, the LLPS process may serve as a key factor in α-Syn oligomerization and aggregation.

Recent findings have highlighted the significant impact of a class of evolutionarily conserved disordered proteins, namely small EDRK-rich factor1a (short isoform) (SERF1a, which will be referred to as "SERF"), on α-Syn toxicity. However, the precise mechanism behind this influence remains unknown. Importantly, SERF can accelerate α-Syn aggregation, specifically within the primary nucleation phase, without perturbing α-Syn activity or integrating into fibrils. This regulatory mechanism stands in contrast to that of molecular chaperones. In response to cellular stress, SERF undergoes rapid release

‡ Co-first author.
* For correspondence: Xiangyan Shi, xyshi@smbu.edu.cn; Yan-Mei Li, liym@mail.tsinghua.edu.cn; Shi-Zhong Luo, luosz@mail.buct.edu.cn.

from the nucleolus and binds with α-Syn in the cytoplasm, generating SERF/α-Syn complexes with highly disordered conformations (32). A biophysical analysis of the SERF/α-Syn complex reveal that its amyloid-promoting activity stems from an early and transient interaction, a key step in α-Syn aggregation. However, the understanding of how the SERF/α-Syn complex formation promotes α-Syn amyloid formation at the molecular level is still lacking.

In this study, we unveil a novel process wherein SERF engages in cophase separation with α-Syn to create fuzzy complexes. The resulting liquid droplets formed by the SERF/α-Syn complexes promote the transition of α-Syn from a soluble to a solid state, while SERF disengages from these droplets, dissolving into the surrounding solution. Furthermore, under conditions relevant to PD, SERF/α-Syn cophase separation occurs, significantly reducing the cytotoxicity caused by the deposition of α-Syn oligomers. In summary, our work sheds light on a previously unexplored mechanism driving the pathological aggregation of α-Syn, which involves cophase separation with SERF, leading to an altered α-Syn aggregation propensity and attenuated capability to form toxic oligomers.

Results

SERF undergoes LLPS driven by electrostatic interaction forces

The conformational anisotropy of the intrinsic structure is considered as a key factor in protein LLPS (33). SERF contains positively charged amino acids and was predicted to possess a highly disordered nature (34) (Fig. 1*A*). To investigate its LLPS capability *in vitro*, we produced recombinant enhanced green fluorescent protein (EGFP)-tagged SERF and examined its LLPS behavior. Liquid droplets were observed at high protein concentration (300 μM) or at a low concentration (30 μM) in the presence of a crowding agent, PEG-8000 (5%) (Fig. 1*B*). The quantification of the dilute phase verified the excluded volume theory predicts (Fig. S7, *C* and *D*). The addition of crowding agents reduced the critical concentration of SERF LLPS (Fig. S1*A*). The analysis of the liquid-like features of SERF phase separation revealed that SERF droplets were stable at a low temperature (4 °C) (Figs. 1*E* and S1, *F* and *J*) and could fuse within 3 s (Fig. 1*C*). The droplets visibly diminished in size after a 2-h incubation at 37 °C and were restored within 2 h by cooling at 4 °C. Fluorescence recovery after photo bleaching (FRAP) assay revealed that SERF molecules could exchange freely in the surrounding dilute solution (Fig. 1*D*), suggesting a high degree of mobility for SERF within the droplets. Subsequently, we overexpressed EGFP-labeled SERF protein and EGFP separately in HeLa cells to determine whether EGFP-SERF could undergo phase separation *in vivo*. Spherical SERF puncta were observed in the nucleus, whereas the singular EGFP label displayed a diffuse distribution (Figs. 1, *F* and *G* and S5*A*), indicating that SERF formed membrane-free condensates in cells. FRAP experiments demonstrated a significant fluorescence recovery of the droplets (Fig. 1*H*). The condensates were numerous and moved slowly in cell nucleus with occasional coalescence (Fig. 1*L*). It appears that SERF is enriched and localized in membraneless organelles such as nucleoli, consistent with previous reports (35).

Given that proteins with repeat sequence of charged amino acids tend to form a concentrated phase due to electrostatic interactions (36), we delved into the role of electrostatic interaction in promoting SERF LLPS. Turbid solutions of SERF formed at low salt concentrations, while elevating the NaCl concentration to 500 mM resulted in a clear solution. The turbidity of the solution reached its peak in the absence of salt and decreased in the high-salt condition (Fig. 1*I*), suggesting that the phase separation of SERF was influenced by electrostatic interactions (37, 38). SERF is rich in lysine and arginine, which is known to interact with RNA (35) (Fig. 1*A*). RNA, due to its linear repetitive structure and abundance of negative charges, has the ability to promote phase separation (39). To validate this, we characterized SERF phase separation in the presence of Poly U, where liquid droplets were observed, becoming more prominent with higher amounts of Poly U. The droplets disassembled when the concentration of Poly U reached to 183.6 μg/ml (Figs. 1*J* and S1*B*). The introduction of RNase led to the dissolution of the droplets (Fig. 1*K*). Poly U appeared to induce SERF droplet formation through electrostatic interactions Furthermore, previous investigations involving mutations at two N-terminal positively charged residues (K17A, K17E, R11E) in SERF demonstrated the critical role of the N-terminal region in SERF-protein interaction (35, 40). In the poly U or 5% PEG-induced phase separation system, wild-type (WT) SERF tended to form larger and more concentrated droplets compared to the mutants (Figs. 1*M* and S1, *C* and *D*). Compared with K17A, K17E and R11E mutants exhibited significantly weaker phase transitions. Those results were consistent with observations in the turbidity experiment (Fig. S1*E*), illustrating the crucial involvement of positively charged amino acids in the SERF droplets formation. Furthermore, experiments were conducted with untagged SERF to eliminate any potential influence of the EGFP tag. These experiments demonstrated that the tag had no impact on SERF droplet formation (Fig. S1, *G–I*). Taken together, phase separation of SERF is primarily mediated by the electrostatic forces, largely governed by its positively charged amino acids.

Solution-state NMR demonstrates that the N-terminal domain of SERF are involved in LLPS

We next implemented solution-state NMR to track changes upon LLPS for SERF at the molecular level. The corresponding protein sequence was shown in Figure 2*A*. The NMR experiments were performed at 25 °C. 2D ^{1}H-^{15}N heteronuclear single quantum coherence (HSQC) spectra were collected for SERF in buffers with various NaCl concentrations (Figs. 2, *B* and *C* and S2*B*). Narrow chemical shift dispersion was observed for peaks in the 2D spectra, which is consistent with the highly disordered structure feature of SERF. The overall structure of SERF remains largely unaltered at different NaCl concentration as evidenced from the absence of considerable chemical shift perturbation. With

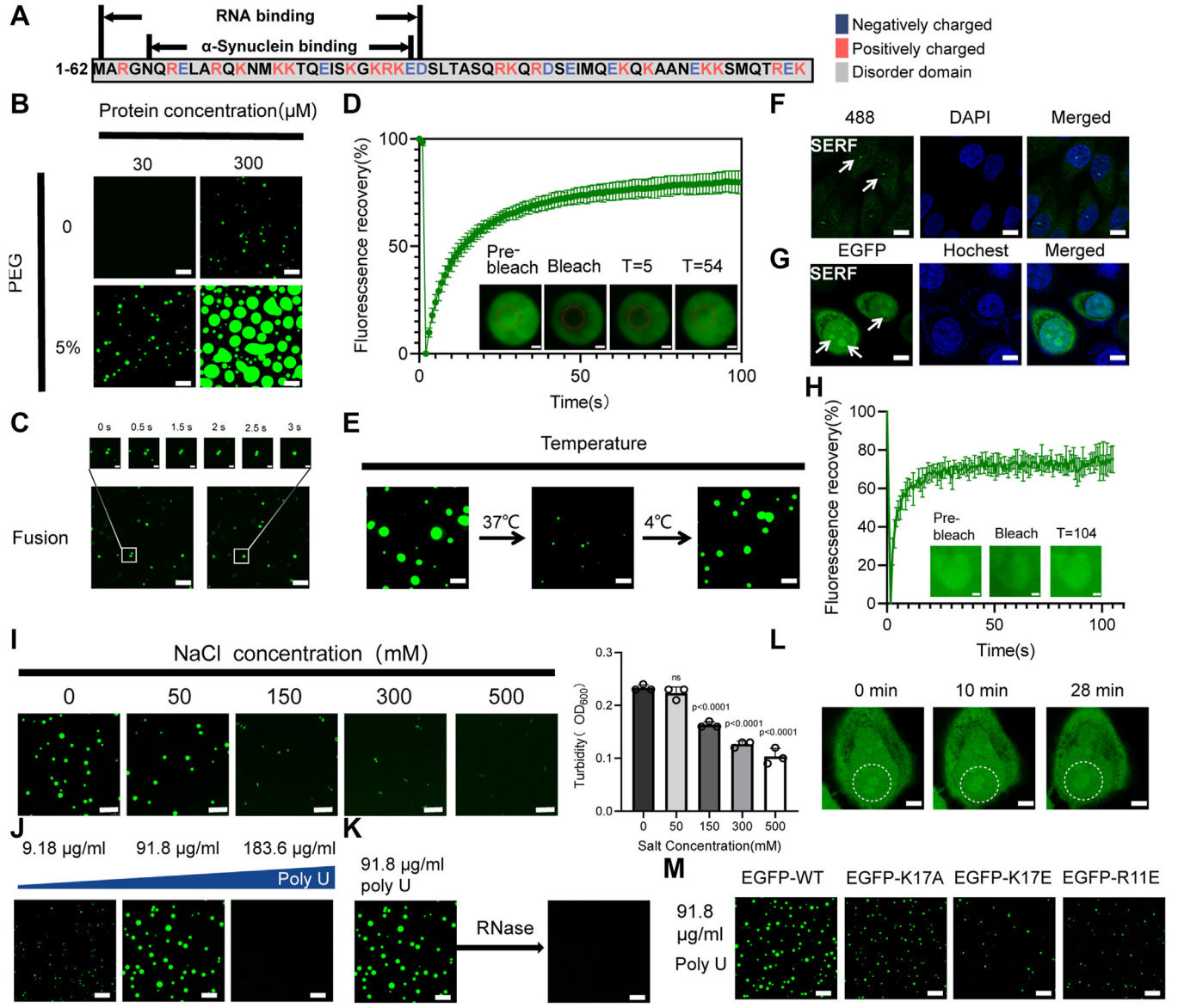

Figure 1. Characterization of SERF LLPS *in vitro* and *in vivo*. *A*, EGFP-SERF sequence shows the α-Syn binding and RNA-binding region. *Letters in blue* indicate negative charge distribution and the positive charge in *red*. *Gray shading* represents disorder domain. *B*, representative confocal microscopy images of EGFP-SERF (*green*) at different protein concentrations in the presence and absence of the molecular crowder PEG-8000. *C*, droplet fusion experiment of 30 μM EGFP-SERF with 5% PEG. The scale bar in the *top row* represents 1 μm. *D*, FRAP of the droplets formed by EGFP-SERF *in vitro* in the presence of 5% PEG. The scale bar represents 2 μm. *E*, confocal microscopy images of EGFP-SERF (30 μM) droplets in the presence of 5% PEG demonstrate the reversible nature of the droplets on heating (37 °C) and cooling (4 °C). Representative images are shown. *F*, confocal microscopy images of the expression of endogenous SERF (*green*) distribution in HeLa cells, respectively. *Arrows*, spot of SERF in cell nucleus. Nuclei are stained with DAPI (*blue*). *G*, confocal microscopy images of the transiently overexpressed EGFP-SERF (*green*) distribution in living HeLa cells, respectively. *Arrows*, spot of SERF in cell nucleus. Nuclei are stained with Hoechst 33342 (*blue*). *H*, FRAP of the condensates formed by SERF in cells. The scale bar represents 1 μm. *I*, *left*: confocal microscopy images of EGFP-SERF (30 μM) at different salt concentrations in the presence of 5% PEG. *Right:* turbidity measurement of SERF with different salt concentrations. ns, not significant, ns = 0.5488. Comparisons among groups were performed using one-way ANOVA with Kruskal–Wallis test or unpaired two-tailed Student's *t* tests with GraphPad Prism 9.0.0. *J* and *K*, confocal microscopy images of liquid droplets formed by EGFP-SERF (30 μM) in the presence of ploy U at different concentrations (*J*), and in the presence or absence RNase of ploy U (91.8 μg/ml) (*K*). The image (*K*, *right*) reuse to show the RNase was added in the same sample. *L*, fusion of two EGFP-SERF assemblies upon contact. The scale bar represents 4 μm. *M*, confocal microscopy images of the droplets formed by WT and mutated-type EGFP-SERF (30 μM) with 91.8 μg/ml ploy U. All the experiments were performed three times with similar observations (*B–L*). Conditions: 20 mM PB pH 7.5. All scale bars represent 10 μm except where noted. α-Syn, α-Synuclein; DAPI, 2-(4-Amidinophenyl)-6-indolecarbamidine dihydrochloride; EGFP, enhanced green fluorescent protein; FRAP, fluorescence recovery after photobleaching; HSQC, heteronuclear single quantum coherence; LLPS, liquid–liquid phase separation; SERF, small EDRK-rich factor.

increasing NaCl concentration from 0 mM to 300 mM, higher peak intensities were detected for a number of peaks in the 2D HSQC spectra. Such alteration of peak intensity with varying NaCl concentration are likely due to the fact that many residues of SERF are involved in intermolecular interactions in the LLPS state (lower NaCl concentration), which reduces their flexibility and leads to decreased peak intensities. Gly residues reside in the N-terminal domain of the protein. The Gly peaks disappeared at low NaCl concentration (0 and 100 mM), suggesting that the N-terminal

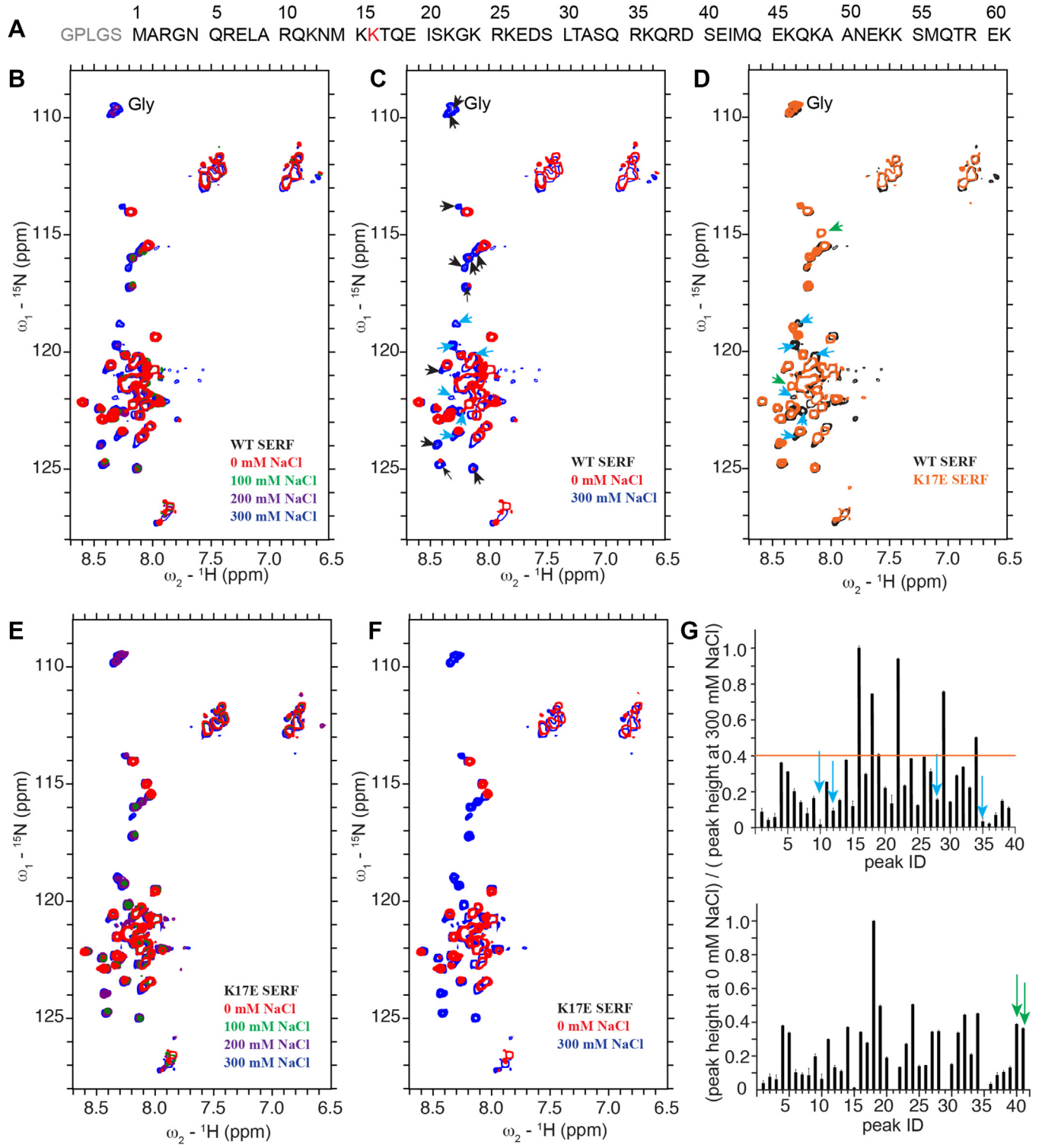

Figure 2. Solution-state NMR characterization of LLPS of WT SERF and K17E SERF. *A*, primary sequence of SERF used in the experiments. Five amino acids were added in the N terminal of the recombinant SERF due to the PreScission protease digestion of GSH-Sepharose affinity chromatography. *B* and *C*, overlaid 2D ^{1}H-^{15}N HSQC spectra of WT SERF in buffers with different NaCl concentrations. *D*, overlaid 2D ^{1}H-^{15}N HSQC spectra of WT SERF and K17E SERF in buffers with 300 mM NaCl. *E* and *F*, overlaid 2D ^{1}H-^{15}N HSQC spectra of K17E SERF in buffers with different NaCl concentrations. *G*, the ratio of normalized ^{1}H-^{15}N HSQC peak intensities of WT SERF at 0 and 300 mM NaCl (*upper*). The ratio of normalized ^{1}H-^{15}N HSQC peak intensities of K17E SERF at 0 and 300 mM NaCl (*lower*). A *horizontal line* is draw to guide visualization. SERF are ^{15}N labeled in the samples. *Cyan arrows* in *C* and *D* mark those showing chemical shift perturbations in the spectrum of K17E mutant in comparison with that of WT SERF. *Arrows* in *B* mark peaks that exhibit significantly attenuated intensities at 0 M NaCl in comparison with that at 300 mM NaCl, among which *cyan arrows* mark the same peaks as displayed in *C*. *Green arrows* mark the peaks that are new in the spectrum of K17E mutant in comparison with that of WT SERF. In G, *cyan and green arrows* mark the same peaks as shown in *D*. In *G*, the ID number of peaks is defined as displayed in Fig. S2, and the profile of peak intensity ration at different NaCl concentrations are presented in Fig. S2. Spectra acquired at 298 K and a protein concentration of 250 μM. α-Syn, α-Synuclein; EGFP, enhanced green fluorescent protein; HSQC, heteronuclear single quantum coherence; LLPS, liquid–liquid phase separation; SERF, small EDRK-rich factor.

domain of SERF participated in the protein–protein interaction in its LLPS.

2D ^{1}H-^{15}N HSQC experiments were next performed for K17E SERF in buffers with 0 to 300 mM NaCl. Similarly, to the WT SERF, decreasing peak intensity were observed for a number of residues in K17E SERF in buffers with lower NaCl concentration due to LLPS (Figs. 2, *E* and *F* and S2*D*). Chemical shift perturbation was detected for a few peaks (cyan arrows) and two new peaks were observed for K17E SERF (green arrows) in comparison with the WT as shown in Figure 2*D*. Those peaks likely belonged to amino acid residues close to K17. Notably, those peaks were among the groups that exhibited significantly attenuated peak intensities for the protein in LLPS state (Fig. 2, *B–F*), which was further verified by the quantified peak intensity profile (Figs. 2*G* and S2, *A* and *C*). Therefore, residues around K17 likely participated in the intermolecular interactions in the protein LLPS state. In fact, among the well-resolved residues, 34 out of 39 possess peak intensities that were significantly attenuated in the spectrum of SERF sample without NaCl (Fig. 2*G*), indicating that the intermolecular interactions in the SERF LLPS state involved at least half the protein.

Cophase separation and aggregation of SERF/α-Syn complex in vitro

Previous studies have highlighted SERF as a direct modulator of amyloid fibril assembly, promoting primary nucleation of amyloids for the α-Syn protein (9, 41). Based on our observations of SERF undergoing LLPS, we hypothesized that SERF promoted the aggregation of α-Syn by facilitating its phase separation. To evaluate this hypothesis, we employed confocal microscopy to detect LLPS in mixtures of SERF (EGFP-fused or 488-stained) and Cy3-stained α-Syn, and monitored thioflavin T (ThT) fluorescence traces for label-free SERF and α-Syn mixtures. As predicted, SERF/α-Syn complex formed liquid droplets with larger size and higher density than the case of SERF alone at equivalent protein concentrations,

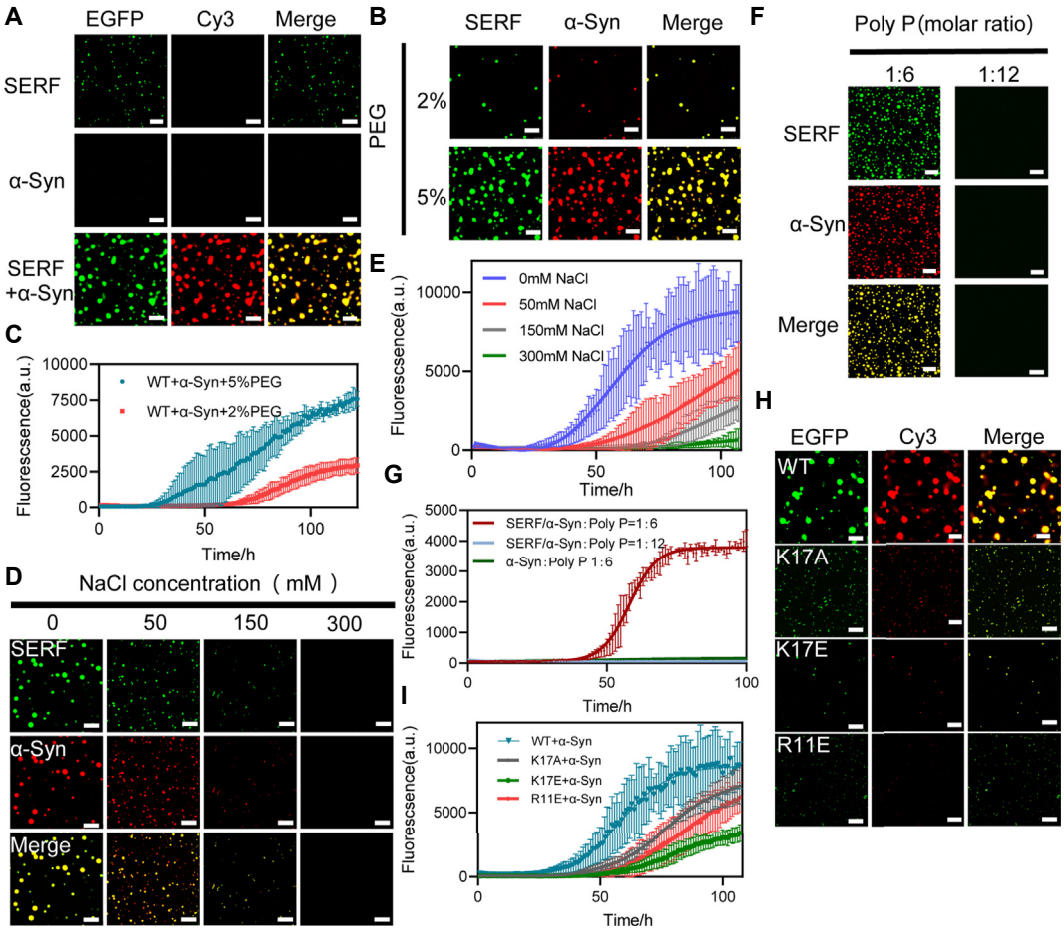

Figure 3. SERF cophase separate with α-Syn *in vitro*. *A*, confocal microscopy images of assembling status of EGFP-SERF, α-Syn, and EGFP-SERF/α-Syn complex liquid droplets (50 μM each). Liquid droplets were imaged immediately. *B* and *C*, confocal microscopy images of EGFP-SERF/α-Syn complex in the PEG concentration (2% and 5%) of liquid droplets (*B*); the ThT fluorescence traces for α-Syn aggregation kinetic under the same condition at 37 °C (*C*), error bars represent SD (n = 3). *D* and *E*, confocal microscopy images of EGFP-SERF/α-Syn complex at different salt concentrations in the presence of 5% PEG (*D*); the ThT fluorescence traces for α-Syn aggregation kinetic under the same condition at 37 °C (*E*), error bars represent SD (n = 3). *F* and *G*, confocal microscopy images of EGFP-SERF/α-Syn complex with Poly P at different ratios (*F*) and the ThT fluorescence traces for α-Syn aggregation kinetic under the same condition at 37 °C (*G*), error bars represent SD (n = 3). *H* and *I*, confocal microscopy images of the complex of WT EGFP-SERF and three mutants combining with α-Syn in the presence of 5% PEG (*H*); the ThT fluorescence traces for α-Syn aggregation kinetic under the same condition at 37 °C (*I*), error bars represent SD (n = 3). All the experiments were performed in the PB buffer pH 7.5. The protein complex system is 50 μM in which the ratio of SERF/α-Syn is 1:1 (50 μM protein, 1:10 ratio of Cy3-labeled α-Syn to unlabeled protein), and all of THT samples was composed of unlabeled SERF. All the image scale bars represent 10 μm. α-Syn, α-Synuclein; EGFP, enhanced green fluorescent protein; SERF, small EDRK-rich factor; ThT, thioflavin T.

while α-Syn proteins did not form droplets (Figs. 3*A* and S4, *A* and *H*). Furthermore, the formation of the droplets was promoted with increasing SERF concentrations in the complex (Fig. S4*E*). Our observations indicate that SERF/α-Syn can undergo cophase separation *in vitro*.

Subsequently, we investigated the kinetics of phase separation and aggregation of SERF/α-Syn system within an environment containing crowding agents. The droplets area of the SERF/α-Syn mixture progressively increased as the PEG concentration was raised from 2% to 5% (Figs. 3*B* and S4*B*). The ThT fluorescence traces were employed to monitor the kinetics of α-Syn fibril formation from the SERF/α-Syn mixture, revealing that robust LLPS (5% PEG) conditions accelerated polymerization and shortened lag phases (Fig. 3*C*). Consequently, a significant accumulation of ThT-reactive species was observed, evident by approximately 3-fold higher ThT fluorescence intensity than the case at the low crowding agent concentration condition (2% PEG). These results collectively suggest that LLPS significantly facilitates SERF/α-Syn interactions, accelerating the formation of aggregates.

To further investigate the SERF/α-Syn cophase separation at the molecular level, we performed solution-state NMR characterization for the SERF/α-Syn system of which SERF was ^{15}N-labeled. The 2D ^{1}H-^{15}N HSQC spectrum of WT SERF/α-Syn was nearly identical to that of WT SERF in the absence of NaCl (Fig. S3, *A*–*C*). This demonstrated that the SERF/α-Syn mixture undergoes LLPS at this condition and the N-terminal domain of SERF participates in the intermolecular interactions. Compared with the spectrum of SERF in the absence of NaCl, a few peaks disappeared in that of SERF/α-Syn, suggesting that α-Syn promotes the LLPS of SERF.

Electrostatic interactions dominate the cophase separation

The stochastic nature of the fuzzy complexes formed by SERF/α-Syn is governed by electrostatic associations (40). We then set out to explore whether the electrostatic interaction is also the driving force behind the cophase separation. As expected, the cophase separation of SERF/α-Syn was hindered as the salt concentration was increased (Figs. 3*D* and S4*C*). Meanwhile, the ThT fluorescence traces showed that LLPS promoted a sharp acceleration of α-Syn fibrillation (Fig. 3*E*). However, inconsistent with the observations that Poly U induced SERF phase separation, the addition of Poly U did not promote the SERF/α-Syn cophase separation (Fig. S4*F*). This phenomenon could potentially be attributed to the fact that both α-Syn and RNA share the same binding sites with SERF at the positively charged N-terminal region (35), thus interfering with the SERF/α-Syn electrostatic associations. Therefore, instead of Poly U, we opted to use polyanionic-Poly P to promote the cophase separation without disrupting SERF/α-Syn interaction. As the molar ratio of the complex to Poly P reached 1:6, SERF/α-Syn exhibited complete colocalization in the droplets (Figs. 3*F* and S4*G*). ThT fluorescence could detect β-pleated sheets of α-Syn at the same condition (Figs. 3*G* and S4*J*). However, excess Poly P directly led to charge imbalance in the solution and resulted in the droplet disassembly.

We further assessed the cophase separation propensity and aggregation behavior of α-Syn with different SERF mutants, for example, R11E mutant showed a similar affinity to α-Syn binding as the WT SERF, while the K17A mutant demonstrated weak interaction and the K17E mutant displayed minimal binding affinity to α-Syn *in vitro* (40). In the presence of crowding agent (5% PEG), all the mutants, of which the positive residues were mutated to negative or neutral residues, processed lower phase separation capability than the WT (Figs. 3*H* and S4*D*), ThT fluorescence analysis revealed a consistent trend between the extent of α-Syn aggregation and the phase separation propensity. Notably, K17A mutant processed a greater capability to promote α-Syn self-assembly than the R11E mutant, despite the latter exhibiting much stronger interaction with α-Syn. In addition, K17E mutant showed unexpected capability to promote α-Syn self-assembly through cophase separation (Fig. 3*I*). These collective findings further support that, rather than relying on the specific strong interactions, it is the weak electrostatic interactions that mediate the SERF/α-Syn cophase separation, ultimately driving α-Syn self-assembly into amyloid fibrils.

Liquid-to-solid phase transition of α-Syn occurs inside complex condensates

To gain deeper insights into the mechanism through which SERF/α-Syn cophase separation triggers α-Syn aggregation, we tracked the dynamic behaviors of the condensates. Upon incubating the SERF/α-Syn complex at 37 °C for varying periods (0, 3, and 7 days), we observed a progression wherein the cophase separation of SERF/α-Syn led to the reversible formation of spherical-shaped condensates at the early stages. These condensates gradually solidified into amorphous structures over time (Fig. 4*A*). The evaluation of proliferation and recovery for each individual protein component by FRAP analysis indicated that SERF exhibited great fluidity and diffusion rates within the condensates, while α-Syn experienced a gradual increase in viscosity, with fluorescent signal recovery becoming undetectable after 3 days (Fig. 4*B*). Remarkably, prolonged incubation resulted in the detachment of SERF from the condensates, leaving α-Syn in a fully solidified state (Figs. 4, *A* and *B*, S4*H*, and S7*B*), which was consistent with previous results that SERF promoted α-Syn aggregation without becoming integrated into α-Syn fibrils (32). Through the LLPS condensates, SERF assisted in the initial nucleation of α-Syn, subsequently detached from the complex system. Meanwhile, α-Syn continued to undergo secondary nucleation, while SERF maintained its high mobility throughout. Our data clearly pointed that α-Syn undergoes a transition from a liquid to a solid state in the SERF/α-Syn cophase separation condensates.

SERF/α-Syn undergoes cophase separation in vivo

To access the cophase separation of SERF/α-Syn *in vivo*, we overexpressed EGFP-SERF (green) and mcherry-α-Syn (red) in HeLa cells, followed by monitoring their cellular localization using confocal microscopy. SERF was observed predominantly in

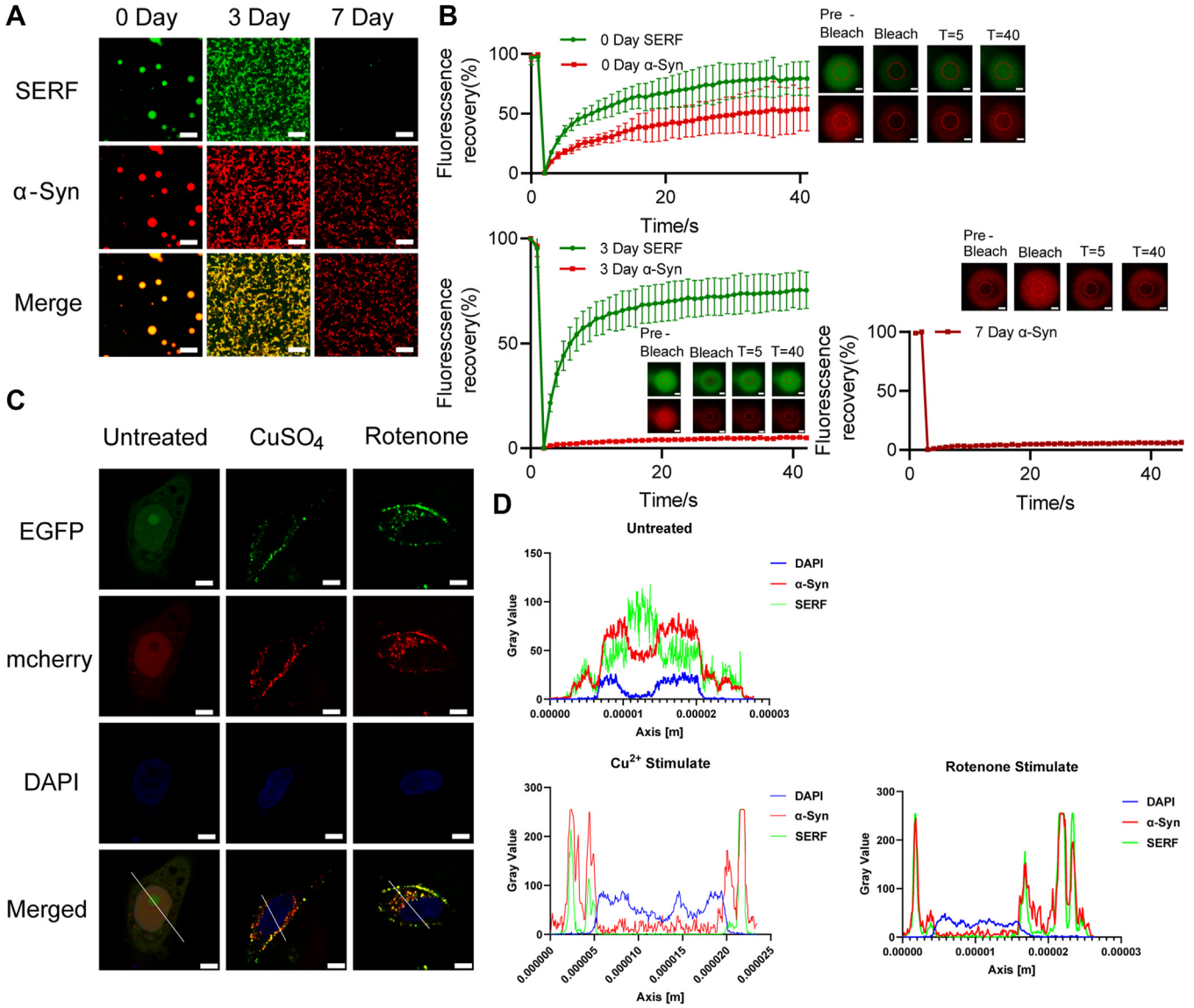

Figure 4. SERF promotes the liquid-to-solid transition of α-Syn to forming amyloid aggregation. *A*, confocal microscopy images of the EGFP-SERF/α-Syn complex (50 μM protein, 1:10 ratio of Cy3-labeled α-Syn to unlabeled protein) incubated for 0, 3, and 7 days at 37 °C. The scale bar represents 10 μm. *B*, FRAP of the condensate formed in condition (*A*). The scale bar represents 1 μm (0 days); and the scale bar represents 500 nm (3 and 7 days). *C*, confocal microscopy images of HeLa cells overexpressing EGFP-SERF (*green*)/mcherry–α-Syn (*red*) complex for 12 h after transfection in the presence or in the absence of 500 nM rotenone or 24 h of 20 μM copper sulfate. *Arrows* point out the spot of SERF, α-Syn, or the merge of them in cell. The scale bar represents 10 μm. *D*, the fluorescence intensity profiles along the indicated *lines* across the complex in (*C*). α-Syn, α-Synuclein; EGFP, enhanced green fluorescent protein; FRAP, fluorescence recovery after photobleaching; SERF, small EDRK-rich factor.

nucleus, whereas α-Syn was distributed in the cytoplasm (Fig. 4*C*). Cotransfection of the two proteins did not affect their separated localization in the cell under native conditions (Figs. 1*E* and S5*B*). Several factors had been recognized as triggers of α-Syn aggregated deposition *in vivo*, such as aging, Cu^{2+}, and rotenone (42, 43). We explored the relationship between these pathological correlates and SERF/α-Syn colocalization. Remarkably, upon treatment with 500 nM rotenone for 12 h or 20 μM copper sulfate for 24 h, SERF/α-Syn showed overlapping in well-defined cytosolic puncta. Line-scanning analysis further confirmed this substantial colocalization (Fig. 4, *C* and *D*). Previous studies reported that the dynamic release of SERF from the nucleolus in the presence of external pressure or disease-related factors, which promoted α-Syn droplet formation in the cell (9, 35). Our findings aligned with these reports, as the cotransfected SERF/α-Syn complexes demonstrated significantly enhanced phase separation in the cellular context (Fig. S5*C*). Intracellular pathological factors triggered nucleocytoplasmic translocation of SERF and the subsequent colocalization of SERF with α-Syn initiated the droplet formation. The nucleus-cytoplasm shuttling under stress conditions may lead SERF to perform such physiological functions.

Oligomers rapidly aggregate into fibrils to attenuate cytotoxicity

The aggregation process of α-Syn monomers could involve a conversion from various soluble polymorphs to insoluble

fibrils. However, the intermediate-state oligomers are widely believed to correlate with the onset of PD pathogenesis. To understand how SERF/α-Syn cophase separation relates to the aggregation state, we examined α-Syn oligomers formation in cell with polyclonal antibody A11 that specifically recognized oligomers of multiple amyloid proteins without binding to the monomers or fibrils. Western blot quantitative analysis revealed that α-Syn oligomers accumulated within 24 h under Cu^{2+} or rotenone stimulation, while the presence of SERF led to the gradual loss of the oligomers and monomers (Fig. 5, *A* and *B*). This suggests that SERF could substantially accelerate the self-assembly of α-Syn *in vivo* under stressful conditions.

Subsequently, we characterized the morphological changes of α-Syn incubated with or without SERF for 0 and 14 days at 37 °C. Western blot quantitative analysis determined that α-Syn monomers gradually transformed into oligomers, and the addition of SERF significantly reduced the accumulation of α-Syn oligomers after 14 days (Fig. S6*A*). Further morphological examination of the polymorphs *via* transmission electron microscopy revealed that α-Syn adopted oligomer-like amorphous aggregates, whereas the SERF/α-Syn complex distinctly yielded filamentous α-Syn fibrils with SERF remaining uninvolved in interactions with aggregating α-Syn (Figs. 5*C* and S6*B*). Fluorescence microscopy characterization revealed the formation of fibril-like aggregates in the SERF/α-Syn complexes as indicated by ThT binding to polymorphs (Fig. 5*C*). Consistent with *in vivo* observations, we demonstrate that SERF can significantly accelerate α-Syn fibrillation and reduce oligomer accumulation.

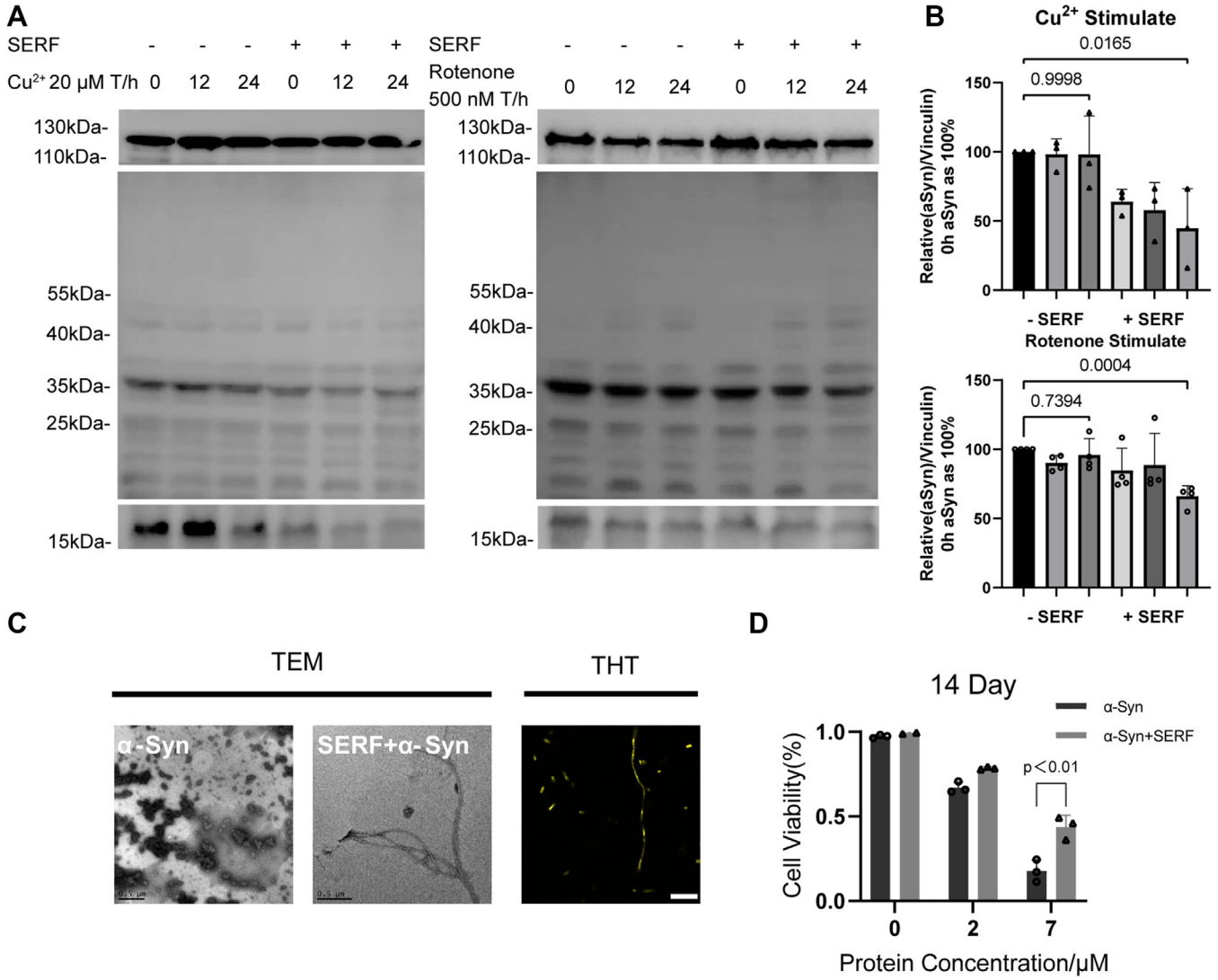

Figure 5. SERF accelerates the step of α-Syn oligomer formation. *A*, Western blot showing α-Syn monomer (*bottom*) and oligomer (*middle*) at different time with or without SERF transfected into the HeLa cells. Then cells were stimulated in the presence of 500 nM rotenone or 20 μM copper sulfate. *B*, quantification of α-Syn monomer in the presence or absence of SERF in (*A*). Comparisons among groups were performed using one-way ANOVA with Kruskal–Wallis test or unpaired two-tailed Student's *t* tests with GraphPad Prism 9.0.0. Error bars represent SD (n = 3). *C*, TEM images of α-Syn with or without the presence of SERF and confocal microscopy image of SERF/α-Syn complex combining with ThT. The scale bar of TEM represents 0.5 μm, and the scale bar of ThT represents 10 μm. All of the samples were incubated without agitation in 20 mM PB, pH 7.5 and 37 °C for 14 days. *D*, viability of HeLa cells measured by CCK8 assay. Fibrils (50 μM) were incubated in the presence or absence of SERF for 24 h at 37 °C and diluted into the cell culture media at the indicated concentrations. Error bars = SD (n = 3). All protein samples were incubated in 20 mM PB, pH 7.5. α-Syn, α-Synuclein; CCK8, cell counting kit-8; SERF, small EDRK-rich factor; TEM, transmission electron microscopy; ThT, thioflavin T.

The toxicity of α-Syn aggregation is a pivotal question in the field of α-Syn–related neurodegenerative research. Increasing number of recent studies suggests that α-Syn oligomers are the more neurotoxic species than the long mature amyloid fibrils. We therefore investigated the effect of SERF on the toxicity of α-Syn oligomers using a cell counting kit-8 (CCK8) assay in HeLa cell model. Equal amounts of α-Syn polymorphs, with or without the presence of SERF, were preincubated for 14 days at 37 °C *in vitro*, and then they were added to the cells to measure the cytotoxicity after 24 h incubation. Combined with the previous data, we revealed that α-Syn oligomers caused a significant inhibition of cell viability in the absence of SERF (approximately 80%, $p < 0.001$), while α-Syn fibrils formed in the presence of SERF performed much less impact (Fig. 5*D*). Thus, we verified that the highly toxic substance of α-Syn was mainly derived from oligomers and the SERF-mediated aggregation of α-Syn reduced the cellular toxicity. Additionally, it is noteworthy that the uptake of these two types of α-Syn mature fibrils resulted in similar levels of endocytosis (Fig. S6*C*). Collectively, these results suggest that SERF promotes the step of α-Syn forming oligomeric intermediates, accelerating the conversion of the protein to fibrils and thus reducing the deposition of toxic α-Syn oligomers.

Discussion

In this work, we reveal that the LLPS property of SERF and SERF/α-Syn complex is closely related to their interaction and biological function (Fig. 6). We elucidate that SERF undergoes LLPS through weak electrostatic interaction forces, and the formation of cophase separation droplets is essential for SERF to promote the α-Syn fibrillation and reduce the oligomer accumulation. The N-terminal domain of SERF is involved in the intermolecular interactions in those LLPS processes. Remarkably, the cophase separation also occurs *in vivo* under pathological stimulation conditions. Importantly,

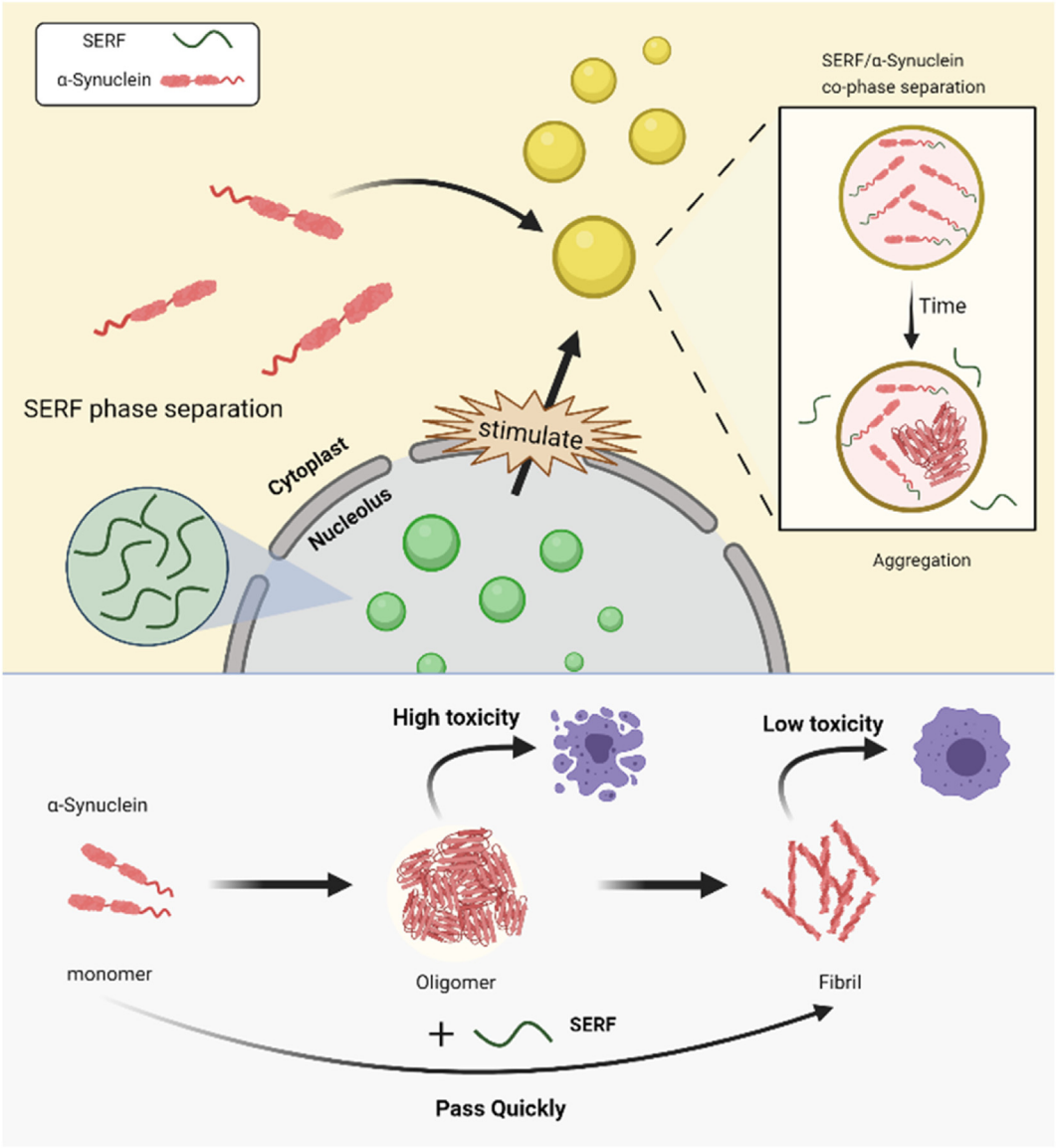

Figure 6. Schematic illustration of the process and function for the SERF/α-Syn cophase separation in the cell.

distinguished from the conventional mechanisms, SERF decreases the α-Syn aggregation toxicity through attenuating the accumulation of the more toxic α-Syn oligomer species, which might serve as a novel mechanism of intracellular self-protection. A recent study (44) suggested that the brain depletion of SERF2 altered the structure of amyloid-β deposits. However, there was no compensatory upregulation of SERF1 in response to SERF2 knockout, which provides a direction for our forthcoming work.

Our work reveals a critical biochemical mechanism related to SERF-phase separation. A previous study reports that SERF potentially assembles fuzzy complexes to accomplish the biological functions including assisting RNA folding in the nucleus and interacting with amyloid in the cytoplasm (35). Herein, we elucidate that this fuzzy complex is assembled *via* a LLPS process. The abundant presence of lysine and arginine residues within SERF plays a significant role in driving the droplet formation. Lacking of the α-helical and β-sheet structural components leads the SERF remaining highly dynamic within the droplets (32, 34). Even a subtle modification of a single positively charged residue in SERF directly impacts the overall charge distribution within the protein, consequently influencing its capacity for undergoing LLPS. Our results reveal that the weak interactions, largely governed by positive charges of SERF, play a central role in driving the phase separation phenomenon.

The amyloid undergoes slow assembly in the condensate, which may be associated with its neurotoxicity. As recently reported, TIA1 mediates cophase separation with tau to accelerate its assembly, resulting in the accumulation of highly cytotoxic oligomers (45). We unveil that LLPS is a key process in the SERF-mediated α-Syn self-assembly. Changing the intermolecular crowding or disrupting the ion balance in solution weakens or disrupts the cophase separation, which can directly block the α-Syn aggregation. Notably, the presence of positive charges on SERF plays an essential role in the droplet formation (46). The introduction of SERF mutations substantially weakened the LLPS capability, subsequently interfering with α-Syn self-assembly. R11E SERF exhibits a significantly stronger interaction with α-Syn than the K17A mutant. Meanwhile, due to the deletion of positive charge that affects the complex cophase separation, K17A SERF surprisingly exhibits heightened propensity to promote α-Syn aggregation relative to the R11E mutant. The N-terminal region of SERF interacts with the acidic C-terminal region of α-Syn (34, 40), which is strongly sensitive to net charge. Weak electrostatic interactions in SERF/α-Syn highlight the unique mechanism of SERF, regulating α-Syn aggregation under LLPS conditions. The SERF/α-Syn cophase separation explains that SERF specifically interacts with α-Syn in the early-stage aggregation, but not in the subsequent assembly process. Within the droplets, SERF maintains a highly flexible conformation, while α-Syn gradually undergoes a transformation from soluble to solid form. Subsequent to the α-Syn primary nucleation, SERF dissociates from the complex, which is consistent with the previous report that SERF specifically accelerates the pre-aggregation of α-Syn without integrating into the fibrils (40).

Our cellular studies demonstrate that the external stimuli, such as copper and rotenone, trigger SERF to shuttle between the nucleus and cytoplasm, causing its colocalization with α-Syn at the cytoplasm, which is similar as the case of stress granules (47). α-Syn oligomers in synucleinopathies form annular pore-like structures, resulting in the permeabilization of lipid bilayers (48). Therefore, modulation of oligomers can be a potentially effective strategy to attenuate α-Syn cytotoxicity. In this study, we describe a unique regulatory mechanism that differs from common molecular chaperones (49, 50). We elucidate that SERF could effectively accelerate the α-Syn fibrosis and concurrently suppress the oligomers accumulation. Our discovery of SERF's ability to diminish the α-Syn oligomer-induced cytotoxicity *via* the LLPS process provides a new perspective to further explore the regulation of amyloid aggregation.

Experimental procedures

Recombinant SERF and α-Syn protein expression and purification

His-EGFP-SERF and SERF WT and mutants including K17A, K17E, and R11E were constructed in pET-28a or pGEX-6P-1 vector. Recombinant plasmid was transformed into *Escherichia .coli* BL21 (DE3) cells that were cultured in LB medium at 37 °C for protein expression. When the culture reached an absorbance (A_{600}) of 0.8 to 1.0, IPTG was added to the culture at a final concentration of 0.5 mM. The cells were further incubated at 16 °C overnight. The His6-tagged protein and GST-tagged protein were purified with *His-trap* chelating column and GSH-*Sepharose* affinity chromatography, separately.

To obtain the His-tagged protein, the cells were harvested by centrifugation, and the pellet was resuspended in in lysis buffer (50 mM Tris, 300 mM NaCl, 10 mM imidazole, 5 mM β-mercaptoethanol, 1 mM PMSF, 1 mg/ml lysozyme, complete Protease Inhibitor cocktail tablet, 1% DNase/RNase mixture). The sample was subject to sonication and then ultracentrifugation, the collected supernatant was loaded onto a Ni-column. The column was first washed with washing buffer (50 mM Tris, 300 mM NaCl, 30 mM imidazole), and the bound protein was eluted with elution buffer (50 mM Tris, 300 mM NaCl, 300 mM imidazole). The fractions containing SERF were pooled, frozen in liquid nitrogen, and stored at −80 °C.

To obtain the GST-tagged protein, the cells were harvested by centrifugation and the pellet was resuspended in lysis buffer (0.01 M phosphate buffer, pH 7.2–7.4, 2 mM DTT, 5 mM β-mercaptoethanol, 1 mM PMSF, 1 mg/ml lysozyme, complete Protease Inhibitor cocktail tablet, 1% DNase/RNase mixture). Upon sonication and ultracentrifugation, the supernatant was obtained and loaded onto a GST-column. The column was then washed and the bound protein was eluted with washing buffer (200 mM NaCl, 25 mM Hepes, pH 7.5, 2 mM DTT). PreScission protease was added to remove the GST-tag over night at 4 °C. SERF fractions were pooled, frozen in liquid nitrogen, and stored at −80 °C.

The purified proteins were validated by SDS-PAGE with Coomassie staining and desalted into the 20 mM sodium-phosphate buffer (pH 7.5) by AKTA pure (General Electric). A260/A280 value is about 0.7 or less. The Agarose Gel Electrophoresis indicated the protein was free of nucleic acid contamination (Fig. S7*A*).

The recombinant WT α-Syn was produced and purified following the method described by Wang *et al.* (51). In brief, α-Syn with no tag was constructed in a pET-22b vector and expressed in *E. coli* BL21 (DE3) cells induced with 1 mM IPTG at 16 °C overnight. After harvesting the cells by centrifugation, the collected cell pellets were treated with osmotic shock buffer (30 mM Tris–HCl, 40% sucrose, and 2 mM EDTA, pH 7.4). After removing the buffer by centrifugation, cells were resuspended in cold water with saturated $MgCl_2$ added. Then the supernatant was collected. Extra precipitation (with HCl to pH 3.5 and NaOH to pH 7 in sequence) was also applied to increase purity. The obtained solution was then purified with RP-HPLC (Shimadzu, LC-20AT; Proteonavi column [Shiseido, 5 μm, 10 × 250 mm]) with a linear gradient of 40 to 70% B for 30 min at a flow rate of 5 ml/min (solvent A: water/0.06% trifluoroacetic acid; solvent B: 80% acetonitrile/20% water/0.06% trifluoroacetic acid). The purified α-Syn was lyophilized for further use.

Fluorescence image acquisition in vitro

Purified proteins were concentrated to 30 to 50 μM and desalted into 20 mM phosphate buffer (16 mM Na_2HPO_4, 4 mM NaH_2PO_4, pH = 7.5). EGFP-SERF (30 μM) was blended with different PEG-8000 concentrations (0%–5%w/v) for SERF phase separation. 30 μM EGFP-SERF was blended with Poly U (0–306.2 mg/ml) in the phosphate buffer for EGFP-SERF-polyanionic condensate formation. The system was measured immediately. Likewise, unlabeled SERF solution involving 5% dyed with Cy3 NHS easter (AAT Bioquest) and 95% undyed protein and the same conditions were used to prepare mixed solutions for imaging. For SERF-α-Syn colocation system, concentration of each protein was 50 μM for phase separation with PEG-8000 (2%–5%) or Poly P (300 mM–600 mM). The mixture solution was incubated in a chamber at 37 °C for subsequent incubation periods. The reaction mixture involved SERF protein (WT, K17A, K17E, R11E) and Cy3 dyed α-Syn. For the α-Syn fibril system, the SERF/α-Syn complex (50 μM) with 20 μM ThT was incubated for 14 days at 37 °C under light-proof conditions. One hundred microliters of the EGFP-SERF and EGFP-SERF-α-Syn mixture reaction were prepared in sundry conditions, including PEG-8000, Poly U, Poly P, ThT at specific concentration. The solutions were drop-casted on 96-well microtiter plate and inspected were visualized with a Zeiss 100 × oil immersion objective in the Leica SP8 confocal microscopy. A field was excited by 100% laser power of a 552-nm or 448-nm laser for colocalization research respectively. Droplet number and area statistics were processed by ImageJ (https://imagej.net/).

Turbidity assay

Protein was prepared as mentioned above. Various concentration of protein (1–50 μM) was mixed with different concentrations of PEG-8000 (5–15%) and Poly U (1–306.2 mg/ml) in the assay. The solution was added into a 384-well plate immediately. Turbidity was measured by absorption at 600 nm by a Spectra Max M2 microplate reader (Molecular Devices) and checked in triplicates (n = 3).

Fluorescence recovery after photobleaching

FRAP assay was confirmed by a Carl Zeiss LSM 780 confocal microscope with a 100 × oil immersion lens. For EGFP-SERF protein *in vitro* and vivo FRAP experiments, photobleaching of the droplets was realized by using 100% laser power of a 488-nm laser. For colocalization mixture, Cy3 signal was bleached by 543-nm laser beam. For each system, the recovery was recorded till the curve stabilizes. The fluorescent intensity of bleached position was computed by Zeiss Zen. The regions of interest intensity at time 0 was defined as 0% and prebleached as 100%. More than three sets of curves were counted to Summary curve by GraphPad prism 8.0 (https://www.graphpad-prism.cn/).

ThT fluorescence assays

The fibrillization reactions were carried out in 20 mM PB buffer (16 mM Na_2HPO_4, 4 mM NaH_2PO_4, pH = 7.5), 20 μM ThT. PEG/NaCl/Poly P was added according to different systems. The fluorescence intensity of ThT (Sigma-Aldrich) was enhanced upon binding to amyloid fibrils. Samples were measured in black 96-well round bottom plates (Corning Costar), three parallels per set. ThT fluorescence changes were monitored at 480 nm, with 440 nm excitation, on a SpectraMax M2 (Molecular Devices). The experiments were carried out at 37 °C with measurements taken at 1-h intervals. Global analysis of α-Syn aggregation kinetics to extract the rate constants for primary nucleation, secondary nucleation, and elongation was performed using the online Amylofit platform (52).

Transmission electron microscopy measurements

The protein samples (α-Syn, SERF/α-Syn) (10 μM) were incubated at 37 °C for 14 days, 10 μl of samples was pipetted onto the carbon-coated copper grid and maintained for 4 min and stained with 2% sodium phosphotungstate acid aqueous solution (pH = 6.5) for 2 min. After the sample drying, the samples were monitored to HT7700 electron microscope (HITACHI) at 100 kV.

^{15}N-labeled SERF preparation for NMR characterization

To obtain ^{15}N-labeled protein, cells were grown in LB at 37 °C until an A_{600} of 0.6 to 0.8 was reached, then centrifuged at low speed, washed with M9 salts (Na_2HPO_4, KH_2PO_4, and NaCl) and resuspended in minimal medium M9 supplemented with $^{15}NH_4Cl$ as the only nitrogen source and grown at 37 °C another 2 h, and then induced with 0.5 mM IPTG at 16 °C. The protein was purified with GSH-*Sepharose* affinity chromatography and the purified proteins were validated by SDS-PAGE.

Solution-state NMR measurements

The solution-state NMR measurements were conducted on a 600 MHz Bruker NMR spectrometer. The SERF were dissolved in 20 mM PB (16 mM Na_2HPO_4, 4 mM NaH_2PO_4, pH = 7.5), 90/10 H_2O/D_2O solution. Multidimensional experiments were performed for SERF or α-Syn with NaCl concentrations of 0.1 to 0.3 mM. The NMR experiments were performed at 25 °C.

Cell culture and transfection assay

HeLa cells (NSTI-BMCR; 1101HUM-PUMC000011) were cultured in the Dulbecco's modified Eagle's medium (DMEM), 10% fetal bovine serum (FBS), and 1% antibiotics (penicillin/streptomycin). The cells were cultured at 37 °C with 5% CO_2 in a humidified incubator. Cell culture and transfection assay. Transfection of SERF attached to the pCDNA3.1-EGFP vector (Miao Ling Plasmid) and α-Syn attached to the CMV-mcherry vector (Beyotime Biotechnology) into cells was performed with Lipo8000 transfection reagent (Beyotime Biotechnology). Cell images were captured with a Leica SP8 confocal microscopy with a 100 × objective (oil immersion).

Immunofluorescence

HeLa cells were grown on glass coverslips for 24 h in complete medium. Remove the growth medium and wash the cells in Dulbecco's PBS (DPBS). Fix for 15 min in 4% formaldehyde (methanol-free) in DPBS and permeabilize for 10 min with 0.1% Triton X-100 in DPBS. Wash with DPBS once and incubate for 1 h at room temperature (RT) in blocking buffer (4% FBS in DPBS) to block nonspecific sites. Incubate the cells overnight at 4 °C with primary antibodies (SERF1A polyclonal antibody, Invitrogen) in blocking buffer. Remove the primary antibodies and rinse the cells briefly in DPBS at the following day. Then wash with DPBS 3 × 10 min. Incubate for 2 h at RT with secondary antibodies (Alexa Fluor 488–labeled goat anti-mouse IgG(H + L), Beyotime) in blocking buffer. Counterstain for 5 min with the nuclear stain 2-(4-Amidinophenyl)-6-indolecarbamidine dihydrochloride (Beyotime). Wash with DPBS 3 × 10 min and sealed with antifluorescence quenching sealing tablets.

Phase separation in vivo

HeLa cell were plastered for 24 h on 8-well dishes at the density of 2.5 to 3 × 104 cells/well and incubated for 24 h after transfection (4 μl transfection reagent (lipo8000 Beyotime), 500 ng plasmid, and 125 μl Opti-MEM medium). For detection of cophase separation of SERF/α-Syn, 20 μM of copper sulphate or 500 nM rotenone was added to induce stress for 12 h. The nucleus was stained with Hoechst 33342 (Beyotime) for 10 min and washed five times with PBS. The cells were examined under a confocal laser scanning microscopy using an inverted Leica SP8 microscope, and imaging was acquired with 100× objective (oil immersion), under 405-nm, 488-nm, and 580-nm excitation. Fluorescence colocalization analysis was performed using ImageJ.

Western blot analysis

HeLa cells were plated on 6-well plates with a density 2 × 10^5 cells/well in 2 ml DMEM supplemented with 10% FBS medium and cultured for 24 h. Then α-Syn, SERF/α-Syn plasmids were transfected into cells and incubated for 24 h. After that, 20 μg/ml of $CuSO_4$ was added into the medium, incubated for 0, 12, and 24 h. Likewise, 500 nM/ml rotenone was added and incubated for 0, 12, 24, and 48 h. Cells were washed three times with PBS, then collected and lysed with radio immunoprecipitation assay lysis buffer (Beyotime Biotechnology). The lysates were centrifuged for 15 min at 12,000 rpm in 4 °C, and the supernatants were detected by Western blotting with indicated antibodies.

Western blot was performed by loading equal amounts of proteins into 12% SDS-PAGE at 300 mA, followed by transfer to polyvinylidene difluoride membranes (Beyotime Biotechnology). After blocking with 5% nonfat dry milk for Western blot for 1 h at RT, the membranes were incubated overnight with either the indicated primary antibodies or biotinylated lectins. After washing, the blots were incubated with the appropriate secondary antibodies. According to the manufacturer's instructions, immunoreactive bands were detected using a BeyoECL Plus kit (Beyotime Biotechnology, P0018S) according to the manufacturer's instructions and the imaging was performed with Chemiscope mini-imaging system (CLINX). To control the protein loading, vinculin antibody (Santa Cruz Biotechnology) was used. The results were analyzed with ImageJ.

Oligomer A11 antibody (Thermo Fisher Scientific) was used for the detection of α-Syn oligomers. Purified mouse α-Syn antibody clone 42 (BD Biosciences) was used for the detection of α-Syn monomer. horse radish peroxidase-labeled Goat Anti-Rabbit IgG and horse radish peroxidase-labeled Goat Anti-mouse IgG (Beyotime Biotechnology) were used as secondary antibody.

Cell proliferation

Cell viability was detected using the CCK-8 assay (Beyotime Biotechnology). For the CCK-8 assay, HeLa Cells were seeded in a 96-well plate (10,000 cell/well/100 uL) in DMEM supplemented with 10% FBS and allowed to adhere for 24 h at 37 °C. Then, the preincubated protein complexes were added to the cells at different concentrations, incubated for 24 h, and measured after adding CCK8 reaction for 4 h. The absorbances were measured at 450 nm. Each group of experiments was repeated three times.

Fibril formation

Two aliquots of 300 μl of α-Syn were prepared from the protein stocks, and diluted in PBS to reach a final concentration of 100 μM. Fibril formation was induced at a concentration of 100 μM α-Syn in the presence or absence of 100 μM SERF under constant shaking (250 rpm) at 37 °C, over 14 days. Prior to cell treatment, the α-Syn fibrils were sonicated for 30 min.

Quantification of the dilute phase

A typical sample of 30 μl was prepared in 20 mM PB (pH 7.5) with varying concentrations of PEG, EGFP-SERF, or SERF as described above. After incubating for 15 to 20 min at RT, the condensed phase was separated from the dilute phase by centrifugation at 21,000*g* for 20 min at RT. The dilute phase was then transferred to a 384-well plate (Nunc, flat-bottomed), and the fluorescence intensity was measured on a SpectraMax M2 (Molecular Devices) at 485/535 nm for SERF or EGFP-SERF. Concentrations of the dilute phase were calculated based on calibration curves.

Cell line treatments with α-Syn

Cells were seeded in 8 well-plate formats. The day after, cells were treated with 10 μM concentrations of α-Syn fibrils for 24 h. At the end of the treatment, cells were extensively washed with PBS and then fixed for 15 min in 4% formaldehyde (methanol-free) in PBS. Then wash with PBS 3 × 10 min and counterstain for 5 min with the nuclear stain 2-(4-Amidinophenyl)-6-indolecarbamidine dihydrochloride (Beyotime) and wash with PBS 3 × 10 min again.

Data availability

All experiments were executed multiple times and independently by different experimentators. The screening and their analyses were performed blindly. No data were excluded from the analyses. Details on quantification are found in Fig legends and in Methods details sections. All results are displayed as means ± SD of the means. All the statistical analyses were performed with GraphPad Prism 9, and the statistical significance was calculated using the unpaired Student's *t* test or one-way ANOVA, followed by Bonferroni or Dunnett post hoc test, depending on the experiments. The statistical test used for each experiment is indicated in the respective Fig legend. Significance is indicated with $^{*}p < 0.05$, $^{**}p < 0.01$, $^{***}p < 0.001$, $^{****}p < 0.0001$, or ns = not significant in the corresponding graphs.

Supporting information—This article contains Supporting information.

Acknowledgments—This work was supported by funding from National Key R&D Program of China (2021YFC2103900), National Natural Science Foundation of China (22261132513, 22277009, 92053108), Joint Project of BRC-BC (Biomedical Translational Engineering Research Center of BUCT-CJFH) (XK2022-07, XK2023-14).

Author contributions—X. S., Y.-M. L., and S.-Z. L. supervision; H.-N. L, T. W, and J.-J. H. methodology; H.-N. L, T. W, J.-J. H., L. C., X. S., Y.-M. L., and S.-Z. L. formal analysis; Y.-M. L. and S.-Z. L. funding acquisition; H.-N. L, T. W, J.-J. H., X. S., Y.-M. L., and S.-Z. L. writing-original draft.

Conflict of interest—The authors declare that they have no conflicts of interest with the contents of this article.

Abbreviations—The abbreviations used are: α-Syn, α-Synuclein; CCK8, cell counting kit-8; DMEM, Dulbecco's modified Eagle's medium; DPBS, Dulbecco's PBS; EGFP, enhanced green fluorescent protein; FBS, fetal bovine serum; FRAP, fluorescence recovery after photobleaching; HSQC, heteronuclear single quantum coherence; LLPS, liquid–liquid phase separation; PD, Parkinson disease; RT, room temperature; SERF, small EDRK-rich factor; ThT, thioflavin T.

References

1. Skachokova, Z., Martinisi, A., Flach, M., Sprenger, F., Naegelin, Y., Steiner-Monard, V., *et al.* (2019) Cerebrospinal fluid from Alzheimer's disease patients promotes tau aggregation in transgenic mice. *Acta Neuropathol. Commun.* **7**, 72
2. Zhang, S., Liu, Y. Q., Jia, C., Lim, Y. J., Feng, G., Xu, E., *et al.* (2021) Mechanistic basis for receptor-mediated pathological α-synuclein fibril cell-to-cell transmission in Parkinson's disease. *Proc. Natl. Acad. Sci. U. S. A.* **118**, e2011196118
3. Zhao, K., Lim, Y. J., Liu, Z., Long, H., Sun, Y., Hu, J. J., *et al.* (2020) Parkinson's disease-related phosphorylation at Tyr39 rearranges α-synuclein amyloid fibril structure revealed by cryo-EM. *Proc. Natl. Acad. Sci. U. S. A.* **117**, 20305–20315
4. Selkoe, D. J., and Hardy, J. (2016) The amyloid hypothesis of Alzheimer's disease at 25 years. *EMBO Mol. Med.* **8**, 595–608
5. Scherzinger, E., Sittler, A., Schweiger, K., Heiser, V., Lurz, R., Hasenbank, R., *et al.* (1999) Self-assembly of polyglutamine-containing huntingtin fragments into amyloid-like fibrils: implications for Huntington's disease pathology. *Proc. Natl. Acad. Sci. U. S. A.* **96**, 4604–4609
6. Ray, S., and Maji, S. K. (2020) Predictable phase-separated proteins. *Nat. Chem.* **12**, 787–789
7. Hofweber, M., and Dormann, D. (2019) Post-translational modifications as regulators of phase separation and RNP granule dynamics. *J. Biol. Chem.* **294**, 7137–7150
8. Alberti, S., and Hyman, A. A. (2016) Are aberrant phase transitions a driver of cellular aging? *BioEssays* **38**, 959–968
9. Ray, S., Singh, N., Kumar, R., Patel, K., Pandey, S., Datta, D., *et al.* (2020) alpha-Synuclein aggregation nucleates through liquid-liquid phase separation. *Nat. Chem.* **12**, 705–716. https://doi.org/10.1038/s41557-020-0465-9
10. Chiti, F., and Dobson, C. M. (2017) Protein misfolding, amyloid formation, and human disease: a summary of progress over the last decade. *Annu. Rev. Biochem.* **86**, 27–68
11. Stephens, A. D., Zacharopoulou, M., Moons, R., Fusco, G., Seetaloo, N., Chiki, A., *et al.* (2020) Extent of N-terminus exposure of monomeric alpha-synuclein determines its aggregation propensity. *Nat. Commun.* **11**, 2820
12. Bassil, F., Brown, H. J., Pattabhiraman, S., Iwasyk, J. E., Maghames, C. M., Meymand, E. S., *et al.* (2020) Amyloid-beta (Aβ) plaques promote seeding and spreading of alpha-synuclein and tau in a mouse model of lewy body disorders with Aβ pathology. *Neuron* **105**, 260–275.e266
13. Chen, S. W., Drakulic, S., Deas, E., Ouberai, M., Aprile, F. A., Arranz, R., *et al.* (2015) Structural characterization of toxic oligomers that are kinetically trapped during α-synuclein fibril formation. *Proc. Natl. Acad. Sci. U. S. A.* **112**, E1994–E2003
14. Viola, K. L., and Klein, W. L. (2015) Amyloid β oligomers in Alzheimer's disease pathogenesis, treatment, and diagnosis. *Acta Neuropathol.* **129**, 183–206
15. Ferreira, D. G., Temido-Ferreira, M., Vicente Miranda, H., Batalha, V. L., Coelho, J. E., Szegö É, M., *et al.* (2017) α-synuclein interacts with PrP(C) to induce cognitive impairment through mGluR5 and NMDAR2B. *Nat. Neurosci.* **20**, 1569–1579
16. Winner, B., Jappelli, R., Maji, S. K., Desplats, P. A., Boyer, L., Aigner, S., *et al.* (2011) In vivo demonstration that alpha-synuclein oligomers are toxic. *Proc. Natl. Acad. Sci. U. S. A.* **108**, 4194–4199
17. Lindersson, E., Beedholm, R., Højrup, P., Moos, T., Gai, W., Hendil, K. B., *et al.* (2004) Proteasomal inhibition by α-synuclein filaments and oligomers. *J. Biol. Chem.* **279**, 12924–12934
18. Castillo-Carranza, D. L., Zhang, Y., Guerrero-Muñoz, M. J., Kayed, R., Rincon-Limas, D. E., and Fernandez-Funez, P. (2012) Differential

activation of the ER stress factor XBP1 by oligomeric assemblies. *Neurochem* **37**, 1707–1717
19. Ludtmann, M. H. R., Angelova, P. R., Horrocks, M. H., Choi, M. L., Rodrigues, M., Baev, A. Y., *et al.* (2018) α-synuclein oligomers interact with ATP synthase and open the permeability transition pore in Parkinson's disease. *Nat. Commun.* **9**, 2293
20. Wood, S. J., Wypych, J., Steavenson, S., Louis, J.-C., Citron, M., and Biere, A. L. (1999) α-Synuclein fibrillogenesis is nucleation-dependent: implications for the pathogenesis of Parkinson's disease. *J. Biol. Chem.* **274**, 19509–19512
21. Klucken, J., Shin, Y., Masliah, E., Hyman, B. T., and McLean, P. J. (2004) Hsp70 reduces α-synuclein aggregation and toxicity. *J. Biol. Chem.* **279**, 25497–25502
22. Luk, K. C., Mills, I. P., Trojanowski, J. Q., and Lee, V. M. (2008) Interactions between Hsp70 and the hydrophobic core of alpha-synuclein inhibit fibril assembly. *Biochemistry* **47**, 12614–12625
23. Tao, J., Berthet, A., Citron, Y. R., Tsiolaki, P. L., Stanley, R., Gestwicki, J. E., *et al.* (2021) Hsp70 chaperone blocks α-synuclein oligomer formation *via* a novel engagement mechanism. *J. Biol. Chem.* **296**. https://doi.org/10.1016/j.jbc.2021.100613
24. Wegmann, S., Eftekharzadeh, B., Tepper, K., Zoltowska, K. M., Bennett, R. E., Dujardin, S., *et al.* (2018) Tau protein liquid-liquid phase separation can initiate tau aggregation. *EMBO J.* **37**, e98049
25. Patel, A., Lee, H. O., Jawerth, L., Maharana, S., Jahnel, M., Hein, M. Y., *et al.* (2015) A liquid-to-solid phase transition of the ALS protein FUS accelerated by disease mutation. *Cell* **162**, 1066–1077
26. Ding, X., Sun, F., Chen, J., Chen, L., Tobin-Miyaji, Y., Xue, S., *et al.* (2020) Amyloid-forming segment induces aggregation of FUS-LC domain from phase separation modulated by site-specific phosphorylation. *J. Mol. Biol.* **432**, 467–483
27. Mukherjee, S., and Panda, D. (2021) Contrasting effects of ferric and ferrous ions on oligomerization and droplet formation of tau: implications in Tauopathies and neurodegeneration. *ACS Chem. Neurosci.* **12**, 4393–4405
28. Riback, J. A., Katanski, C. D., Kear-Scott, J. L., Pilipenko, E. V., Rojek, A. E., Sosnick, T. R., *et al.* (2017) Stress-triggered phase separation is an adaptive, evolutionarily tuned response. *Cell* **168**, 1028–1040.e19
29. Xue, S., Gong, R., He, F., Li, Y., Wang, Y., Tan, T., *et al.* (2019) Low-complexity domain of U1-70K modulates phase separation and aggregation through distinctive basic-acidic motifs. *Sci. Adv.* **5**, eaax5349
30. Haass, C., and Selkoe, D. J. (2007) Soluble protein oligomers in neurodegeneration: lessons from the Alzheimer's amyloid β-peptide. *Nat. Rev. Mol. Cell Biol.* **8**, 101–112
31. Fusco, G., Chen, S. W., Williamson, P. T. F., Cascella, R., Perni, M., Jarvis, J. A., *et al.* (2017) Structural basis of membrane disruption and cellular toxicity by α-synuclein oligomers. *Science* **358**, 1440–1443
32. Meinen, B. A., Gadkari, V. V., Stull, F., Ruotolo, B. T., and Bardwell, J. C. A. (2019) SERF engages in a fuzzy complex that accelerates primary nucleation of amyloid proteins. *Proc. Natl. Acad. Sci. U. S. A.* **116**, 23040–23049
33. Brangwynne, C. P., Tompa, P., and Pappu, R. V. (2015) Polymer physics of intracellular phase transitions. *Nat. Phys.* **11**, 899–904
34. Falsone, S. F., Meyer, N. H., Schrank, E., Leitinger, G., Pham, C. L., Fodero-Tavoletti, M. T., *et al.* (2012) SERF protein is a direct modifier of amyloid fiber assembly. *Cell Rep.* **2**, 358–371
35. Meyer, N. H., Dellago, H., Tam-Amersdorfer, C., Merle, D. A., Parlato, R., Gesslbauer, B., *et al.* (2020) Structural fuzziness of the RNA-organizing protein SERF determines a toxic gain-of-interaction. *J. Mol. Biol.* **432**, 930–951
36. Roden, C., and Gladfelter, A. S. (2021) RNA contributions to the form and function of biomolecular condensates. *Nat. Rev. Mol. Cell Biol.* **22**, 183–195
37. Krainer, G., Welsh, T. J., Joseph, J. A., Espinosa, J. R., Wittmann, S., de Csillery, E., *et al.* (2021) Reentrant liquid condensate phase of proteins is stabilized by hydrophobic and non-ionic interactions. *Nat. Commun.* **12**, 1085
38. Li, W., Hu, J., Shi, B., Palomba, F., Digman, M. A., Gratton, E., *et al.* (2020) Biophysical properties of AKAP95 protein condensates regulate splicing and tumorigenesis. *Nat. Cell Biol.* **22**, 960–972
39. Maharana, S., Wang, J., Papadopoulos, D. K., Richter, D., Pozniakovsky, A., Poser, I., *et al.* (2018) RNA buffers the phase separation behavior of prion-like RNA binding proteins. *Science* **360**, 918–921
40. Merle, D. A., Witternigg, A., Tam-Amersdorfer, C., Hartlmuller, C., Spreitzer, E., Schrank, E., *et al.* (2019) Increased aggregation tendency of alpha-synuclein in a fully disordered protein complex. *J. Mol. Biol.* **431**, 2581–2598
41. van Ham, T. J., Holmberg, M. A., van der Goot, A. T., Teuling, E., Garcia-Arencibia, M., Kim, H. E., *et al.* (2010) Identification of MOAG-4/SERF as a regulator of age-related proteotoxicity. *Cell* **142**, 601–612
42. Dadakhujaev, S., Noh, H. S., Jung, E. J., Cha, J.-Y., Baek, S. M., Ha, J. H., *et al.* (2010) Autophagy protects the rotenone-induced cell death in α-synuclein overexpressing SH-SY5Y cells. *Neurosci* **472**, 47–52
43. Binolfi, A., Rasia, R. M., Bertoncini, C. W., Ceolin, M., Zweckstetter, M., Griesinger, C., *et al.* (2006) Interaction of α-synuclein with divalent metal ions reveals key differences: a link between structure, binding specificity and fibrillation enhancement. *J. Am. Chem. Soc.* **128**, 9893–9901
44. Stroo, E., Janssen, L., Sin, O., Hogewerf, W., Koster, M., Harkema, L., *et al.* (2023) Deletion of SERF2 in mice delays embryonic development and alters amyloid deposit structure in the brain Life. *Sci. Alliance* **6**. https://doi.org/10.26508/lsa.202201730
45. Ash, P. E. A., Lei, S., Shattuck, J., Boudeau, S., Carlomagno, Y., Medalla, M., *et al.* (2021) TIA1 potentiates tau phase separation and promotes generation of toxic oligomeric tau. *Proc. Natl. Acad. Sci. U. S. A.* **118**, e2014188118
46. Banani, S. F., Lee, H. O., Hyman, A. A., and Rosen, M. K. (2017) Biomolecular condensates: organizers of cellular biochemistry. *Nat. Rev. Mol. Cell Biol.* **18**, 285–298
47. Daigle, J. G., Krishnamurthy, K., Ramesh, N., Casci, I., Monaghan, J., McAvoy, K., *et al.* (2016) Pur-alpha regulates cytoplasmic stress granule dynamics and ameliorates FUS toxicity. *Acta Neuropathol.* **131**, 605–620
48. Kostka, M., Hogen, T., Danzer, K. M., Levin, J., Habeck, M., Wirth, A., *et al.* (2008) Single particle characterization of iron-induced pore-forming alpha-synuclein oligomers. *J. Biol. Chem.* **283**, 10992–11003
49. Hartl, F. U. (2017) Protein misfolding diseases. *Annu. Rev. Biochem.* **86**, 21–26
50. Yu, H., Lu, S., Gasior, K., Singh, D., Vazquez-Sanchez, S., Tapia, O., *et al.* (2021) HSP70 chaperones RNA-free TDP-43 into anisotropic intranuclear liquid spherical shells. *Science* **371**, eabb4309
51. Huang, C., Ren, G., Zhou, H., and Wang, C.-c. (2005) A new method for purification of recombinant human α-synuclein in Escherichia coli. *Protein Expr. Purif.* **42**, 173–177
52. Meisl, G., Kirkegaard, J. B., Arosio, P., Michaels, T. C. T., Vendruscolo, M., Dobson, C. M., *et al.* (2016) Molecular mechanisms of protein aggregation from global fitting of kinetic models. *Nat. Protoc.* **11**, 252–272